PHYSICAL REVIEW D **88,** 094019 (2013)

Elastic pp scattering from the optical point to past the dip: An empirical parametrization from ISR to the LHC

D. A. Fagundes*
INFN Frascati National Laboratories, Via E. Fermi 40, 00444, Italy and Instituto de Física Gleb Wataghin, Universidade Estadual de Campinas, UNICAMP, 13083-859 Campinas SP, Brazil

G. Pancheri†
INFN Frascati National Laboratories, Via E. Fermi 40, 00444, Italy

A. Grau‡
Departamento de Física Teórica y del Cosmos, Universidad de Granada, 18071 Granada, Spain

S. Pacetti§ and Y. N. Srivastava‖
Physics Department and INFN, University of Perugia, 06123 Perugia, Italy
(Received 13 June 2013; published 26 November 2013)

We describe the main features of recent LHC data on elastic pp scattering through a simple parametrization to the amplitude, inspired by a model proposed by Barger and Phillips in 1973, comprised of two exponentials with a relative phase. Despite its simplicity, this parametrization reproduces two essential aspects of the elastic differential cross section: the well-known precipitous descent in the forward direction and a sharp "dip" structure. To include a complete description of data sets near $-t = 0$, we correct the original parametrization. We examine two possibilities: the presence of the two-pion threshold singularity or a multiplicative factor reflecting the proton form factor. We find good descriptions of LHC7 and ISR data in either case. The form-factor model allows simple predictions for higher energies through asymptotic theorems and asymptotic sum rules in impact parameter space. We present predictions for this model at higher LHC energies, which can be used to test whether asymptotia is reached. The black-disk limit in this model is seen to be reached only for $\sqrt{s} \sim 10^6$ TeV.

DOI: 10.1103/PhysRevD.88.094019 PACS numbers: 13.75.Cs, 13.85.−t

I. INTRODUCTION

The total pp cross section and the elastic differential cross section offer a unique opportunity to study confinement and the transition to perturbative QCD, as they are influenced by large and small distances.

We now have data for the total and the elastic differential cross section from LHC running at $\sqrt{s} = 7$ TeV (LHC7) [1]. Data from LHC running at $\sqrt{s} = 8$ TeV (LHC8) [2] are available for the total cross section, and are expected soon for the differential cross section. We notice that data at $\sqrt{s} = 14$ TeV (LHC14) may be, for a long time, our last chance to study pp scattering and explain it in fundamental terms. A tool to help in this endeavor is a good phenomenological understanding of the data, without the bias imposed by models. To present one such phenomenological description is the aim of this paper.

In what follows we shall propose an empirical description of the differential elastic pp cross section to be used at LHC8 and LHC14. This description follows from the original proposal by Barger and Phillips (BP) [3], who described ISR data with a five-parameter fit, i.e. writing the scattering amplitude as

$$\mathcal{A}(s,t) = i[\sqrt{A(s)}e^{B(s)t/2} + e^{i\phi(s)}\sqrt{C(s)}e^{D(s)t/2}]. \quad (1)$$

In Ref. [4], we had applied this parametrization to preliminary TOTEM results at LHC7 for the elastic differential cross section [5]. In this paper we refine that analysis by presenting an improved description of published data [1], which includes the very small $-t$ value, i.e. parametrizing both the total and the elastic cross section within a few percent of the present LHC7 data.

The idea in the present paper, as in our previous one [4], is to dissect the elastic differential cross section into its basic building blocks—namely the optical point, the forward peak, the dip and the tail—and study the energy dependence of each of them in a single simple analytical expression. We hope in this way to gain insight on a problem which has so far defied a complete description. We find that the optical point requires the introduction of the proton form factor, and we modify Eq. (1) accordingly.

The energy dependence of the parameters in this model is *a priori* unknown. However, asymptotic theorems can be invoked for a possible extension of the model to higher energies. In particular, since the parameters A and B

*fagundes@ifi.unicamp.br
†giulia.pancheri@lnf.infn.it
‡igrau@ugr.es
§simone.pacetti@pg.infn.it
‖yogendra.srivastava@pg.infn.it

control the total cross section and the diffractive peak, we use the Froissart-Martin bound [6,7] and unitarity to propose an expression for their energy dependence. For the second term, which is nonleading at small $-t$-values, we use the Khuri-Kinoshita theorem [8] and total absorption in impact parameter space at infinite energy [4]. While this procedure introduces more parameters, it also clarifies the role played by each term in Eq. (1) and allows us to study the black-disk limit. We shall show that, with this parametrization, the black-disk limit is only obtained for energies well beyond the reach of present-day cosmic-ray or accelerator experiments.

II. THE BARGER AND PHILLIPS MODEL AND LHC7 DATA

The parametrization, given in Eq. (1), corresponds to a complex amplitude, which is composed of two terms, and a relative phase ϕ, which was found phenomenologically to be $\sim$2.8 rad at LHC7, and can be interpreted as corresponding to contributions from opposite parities, $C = \pm 1$. The publication of the actual data by the TOTEM collaboration [1] requires an update and also a revision of the analysis we performed to preliminary TOTEM data in Refs. [4,9]. Applying Eq. (1) to the published data and using the same parameters as in Ref. [4], we find that, when both statistical and systematic errors are included in the fit, the description is still acceptable with $\chi^2/\text{d.o.f.} \sim 2.6$. However, when the analysis is performed with only statistical errors, the χ^2 for the entire range becomes unacceptably large. In particular, the parametrization of Eq. (1) reproduces poorly the measured value of the total cross section at LHC7. The problem therefore seems to lie with the optical point. To pinpoint the origin of the problem, we have fitted TOTEM LHC7 data [1] by implementing different cuts of $t_{\min}$ for which the BP model provides a suitable description. Specifically, any result with $\chi^2/\text{d.o.f.} \lesssim 3$ is considered acceptable. In Table I we display a grid of possible cuts and the respective $\chi^2/\text{d.o.f.}$ values. We also calculate the corresponding values obtained for the differential cross section at the optical point and the total cross section. We find that, when the fit with the BP amplitude is able to reproduce the optical point, the statistical description is not very good. On the other hand, the fit becomes quite good for $0.2\ \text{GeV}^2 < |t_{\min}| < 0.3\ \text{GeV}^2$, even though the total cross section obtained in these cases is too low. From Table I we conclude that, past the very small $-t < 0.2\ \text{GeV}^2$ values, the parametrization of Eq. (1) is suitable to describe two essential features of the differential elastic cross section at high energies, namely the dip structure and the larger $|t|$ region, as one can also see from Fig. 1. Notice that the exponential fit in the range $|t| > 1.0\ \text{GeV}^2$ can be taken to be as good as the power-law fit $|t|^{-n}$ presented by the TOTEM Collaboration in Ref. [5]. This is shown in the inset of Fig. 1 where we display both fits in the large $-t$ range, following TOTEM's fit procedure, namely, taking only the data in the range $1.5\ \text{GeV}^2 < -t < 2.0\ \text{GeV}^2$. In this sense, the comparison with their fit is immediate. We notice at this point that, for the BP model of Eq. (1) to give a good global description from the optical point to past the dip, the very small $|t|$ behavior must receive a correction, while, at the same time, the region past $-t = 0.2\ \text{GeV}^2$ should still be described through two exponentials (and the phase). Namely, since the BP model gives a very good description of LHC7 data except that in the forward region, there is no phenomenological reason to modify it either around the dip or in the tail. We thus propose to ameliorate the very small $-t$ behavior by modifying only the first term in Eq. (1) with a factor $G(s,t)$ such that $G(s,0) = 1$, and suggest to parametrize existing and future pp data with the amplitude

$$\mathcal{A}(s,t) = i[G(s,t)\sqrt{A(s)}e^{B(s)t/2} + e^{i\phi(s)}\sqrt{C(s)}e^{D(s)t/2}]. \quad (2)$$

We have examined two possibilities:

(i) A factor $G(s,t) = \exp[-\gamma(s)(\sqrt{4\mu^2 - t} - 2\mu)]$ reflecting the presence of the nearest t-channel singularity, i.e. the two-pion threshold [10,11]

TABLE I. Statistical results of fits to TOTEM data for the elastic differential pp cross section at LHC7 [1] with the simple BP model of Eq. (1), with χ^2 calculated for the range $-t > -t_{\min}$ and the resulting values for the optical point and the total cross section.

$-t_{\min}$ (GeV^2)	d.o.f.	χ^2/d.o.f.	$d\sigma_{\text{el}}/dt\|_{t=0}$ (mbGeV^{-2})	σ_{tot} (mb)
0.01	156	9.40	490.2	97.9
0.10	118	6.33	422.8	90.9
0.20	94	2.66	282.0	74.2
0.30	80	1.62	181.8	59.6
0.40	70	1.41	212.1	64.4

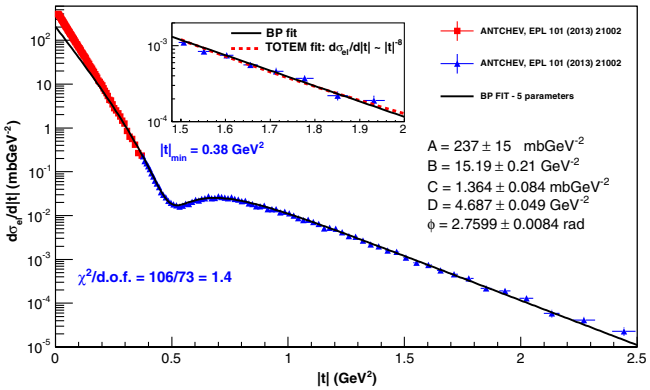

FIG. 1 (color online). Fit to the differential pp cross section at 7.0 TeV [1] with the BP parametrization of Eq. (1) in the range $0.38 \le |t| \le 2.4\ \text{GeV}^2$ with $\chi^2/\text{d.o.f.}$ in this interval. Inset: The power-law fit $|t|^{-n}$, with $n \approx 8$, compared to the exponential fit in the range $1.5 \le |t| \le 2.0\ \text{GeV}^2$.

discussed in Refs. [12,13]; this possibility is labelled the $mBP1$ model,

(ii) A factor $G(s,t) = F_P^2 = 1/(1 - t/t_0)^4$ modeled after the proton form factor, which describes phenomenologically the probability that the proton breaks up as the squared momentum transfer increases; this is labelled the $mBP2$ model.

The $mBP1$ model and other possible modifications of the BP models are discussed in detail in Appendices A and B. In the appendices we shall also present further details, such as analytic expressions for the elastic cross section and, in Appendix C, the impact parameter profile functions for both the $mBP1$ and $mBP2$ models.

III. THE PROTON FORM-FACTOR MODIFICATION: $mBP2$

In this section, and the ones to follow, we present a modification of the BP model at very small t values obtained through the proton form factor. As a viable parametrization of LHC data, we analyze the physics content of the following model for the elastic scattering amplitude:

$$\mathcal{A}(s,t) = i[F_P^2(t)\sqrt{A(s)}e^{B(s)t/2} + e^{i\phi(s)}\sqrt{C(s)}e^{D(s)t/2}], \quad (3)$$

with A, B, C, D, ϕ and t_0 as free parameters. We display our results with this model (henceforth called $mBP2$) in Fig. 2. ISR data sets used in the fits comprise the data collection by Amaldi and Schubert [14] and all experimental information available from 1980 onwards [15–18]. LHC7 data are from Ref. [1].

A point to notice is that at the ISR energy $\sqrt{s} =$ 53 GeV, the data beyond $-t \simeq 7$ GeV^2 suggest the presence of a second wiggle in the amplitude, as would be expected by simple eikonal models. In this range the present parametrization does not reproduce this behavior. Data are scant here, but it is also possible for the parametrization not to hold for the entire $-t$ range explored at ISR. Namely no conclusion can be drawn about the validity of the model at ISR beyond $-t \simeq 7$ GeV^2. On the other hand, no second wiggle is seen at higher energies in the TOTEM data and the increase with energy of the slope $D(s)$ (see Table II) could cover any wiggle beyond the first dip. This is a specific prediction of this model, in this $|t|$ range.

Another comment still concerns the tail at LHC7. In this model, the large $-t$ behavior is described by an exponential with the slope $D(s)$. This differs from the power-law behavior proposed by the TOTEM collaboration [1]. A similar power law was also proposed by Barger and Phillips in Ref. [3] and could be ascribed to a large $-t$ proton form-factor behavior. A QCD interpretation as a triple-gluon exchange was proposed in Refs. [19,20]. Our proposal follows the empirical scope of this and our previous paper [4] in providing a parametrization for the entire $-t$ range under consideration. Figure 2 shows the two fits,

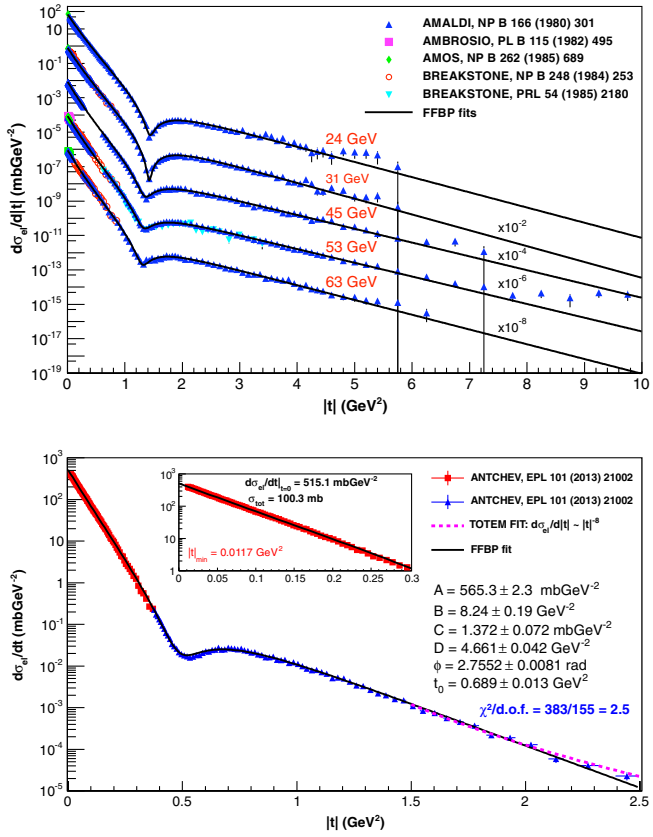

FIG. 2 (color online). Fits to the ISR and LHC7 data sets with the model $mBP2$, and with t_0 a free parameter. Data sets are as described in the text. Inset: LHC7 data near the optical point are shown in comparison with the present model, which includes the proton form-factor modification.

TOTEM and ours, extrapolated up to $-t = 2.5$ GeV^2 and highlights both fits outside the narrow range 1.5 GeV^2 $< -t <$ 2.0 GeV^2.

We summarize the results of the fit in Table II, while plots and fit results for the model with the two-pion threshold correcting the $t \sim 0$ behavior can be found in Appendix A. From this table we notice that the value of the parameter t_0 is larger at ISR energies than at LHC7, where its value is consistent with $F_P(t)$ being the electromagnetic (EM) form factor, i.e. $t_0 \sim 0.71$ GeV^2. Namely, it would appear that asymptotically, t_0 corresponds to its EM form factor value. In fact, fits to the LHC7 data with this value give a χ^2/d.o.f. $= 2.5$ just as in the case of the free fit. This difference between ISR and LHC probably corresponds to low-energy contributions to this parameter. We reproduce this result in the last two rows, which correspond to the fit to LHC7 data obtained by using for t_0 the results from the fit (six-parameter fit) or keeping t_0 fixed at 0.71 GeV^2 (five-parameter fit).

From the $mBP2$ model the analytical expression for the elastic cross section is

TABLE II. The first six rows give values of the free-fit parameters A, B, C, D, t_0 and ϕ for the model $mBP2$ at each energy analyzed. In the last row, the scale parameter t_0 is kept fixed. A and C are expressed in units mbGeV^{-2}, B and D in units of GeV^{-2}, t_0 in units of GeV^2 and ϕ in radians.

$\sqrt{s}$ (GeV)	A	B	$C(\times 10^{-3})$	D	t_0	ϕ	d.o.f.	$\frac{\chi^2}{\text{d.o.f.}}$
24	74.8 ± 0.8	4.0 ± 0.1	4.8 ± 0.7	2.03 ± 0.06	1.06 ± 0.03	3.31 ± 0.01	128	1.2
31	83.7 ± 0.2	3.90 ± 0.07	5.4 ± 0.5	2.12 ± 0.04	0.99 ± 0.01	3.06 ± 0.01	200	1.6
45	89.6 ± 0.2	4.27 ± 0.05	2.4 ± 0.2	1.84 ± 0.02	0.912 ± 0.009	2.83 ± 0.01	201	3.7
53	93.0 ± 0.1	4.51 ± 0.05	2.5 ± 0.1	1.84 ± 0.01	0.947 ± 0.008	2.79 ± 0.01	313	4.7
63	97.4 ± 0.2	4.3 ± 0.1	3.5 ± 0.4	1.97 ± 0.04	0.90 ± 0.01	2.86 ± 0.06	159	2.1
7000	565 ± 2	8.2 ± 0.2	1370 ± 70	4.66 ± 0.04	0.69 ± 0.01	2.755 ± 0.008	155	2.5
7000	562 ± 1	8.54 ± 0.03	1280 ± 34	4.61 ± 0.03	0.71 (fixed)	2.744 ± 0.004	156	2.5

$$\sigma_{\rm el}(s) = A t_0 e^{Bt_0} E_8(Bt_0) + \frac{C}{D} + 2(\sqrt{AC}\cos\phi) t_0 e^{(B+D)t_0/2} E_4\left(\frac{(B+D)t_0}{2}\right), \quad (4)$$

with $E_n(x) = \int_1^\infty dy e^{-xy}/y^n$. In Table III we present the values of the total and elastic cross sections as obtained from both models, $mBP1$ and $mBP2$, together with the optical point for LHC7 and ISR energies. Parameter values for the $mBP1$ model can be found in Appendix A.

We shall now apply to the modified amplitude the asymptotic sum rules presented in our previous analysis [4]. The sum rules correspond to the ansatz of total absorption in b space, namely, $SR_1 \equiv \Im m \tilde{\mathcal{A}}(s, b=0) = 1$ and $SR_0 \equiv \Re e \tilde{\mathcal{A}}(s, b=0) = 0$ at asymptotic energies, where $\tilde{\mathcal{A}}(b, s)$ is the Fourier transform of the scattering amplitude in b space. For the $mBP1$ model, the analytical expressions for the sum rules for the imaginary and real parts of the amplitude are presented in Appendix A. As discussed in Ref. [4], for the satisfaction of the first sum rule, $SR_0 = 0$, it is necessary to introduce a real part for the first term, the one dominant at small $-t$, for which $C = +1$. Let us denote with $\hat{\rho}(s)$ the contribution to the ratio of the real part to the imaginary part of the first term. For $mBP2$ the sum rules give the following results:

$$SR_1 = \frac{1}{2\sqrt{\pi}} \int_o^\infty dT \left[\sqrt{\frac{A}{1+\hat{\rho}^2}} \frac{e^{-BT/2}}{[1+(T/t_0)]^4} - \sqrt{C} e^{-DT/2} |\cos\phi| \right] = \frac{1}{\sqrt{\pi}} \left[-\frac{\sqrt{C}}{D} |\cos\phi| + \sqrt{\frac{A}{1+\hat{\rho}^2}} \frac{t_0}{2} e^{Bt_0/2} E_4(Bt_0/2) \right], \quad (5)$$

$$SR_0 = \frac{1}{\sqrt{\pi}} \left[-\frac{\sqrt{C}}{D} \sin\phi + \sqrt{\frac{A}{1+\hat{\rho}^2}} \hat{\rho} \frac{t_0}{2} e^{Bt_0/2} E_4(Bt_0/2) \right]. \quad (6)$$

Using the tight bound

$$\frac{1}{x+n} < [e^x E_n(x)] < \frac{1}{x+n-1}; \qquad n = 1, 2, \ldots, \quad (7)$$

we have

$$\left[\frac{1}{B + 8/t_0}\right] < \frac{t_0}{2} e^{Bt_0/2} E_4(Bt_0/2) < \left[\frac{1}{B + 6/t_0}\right]. \quad (8)$$

Hence, a simple analytical result for the sum rules can be obtained in the modified $mBP2$ model by taking the mean value 7 in the denominator, so that

$$SR_1 = \frac{1}{\sqrt{\pi}} \left[-\frac{\sqrt{C}}{D} |\cos\phi| + \frac{\sqrt{\frac{A}{1+\hat{\rho}^2}}}{\hat{B}} \right]; \qquad \hat{B} = B + \frac{7}{t_0}, \quad (9)$$

$$SR_0 = \frac{1}{\sqrt{\pi}} \left[-\frac{\sqrt{C}}{D} \sin\phi + \frac{\sqrt{\frac{A}{1+\hat{\rho}^2}}}{\hat{B}} \hat{\rho} \right]; \qquad \hat{B} = B + \frac{7}{t_0}. \quad (10)$$

Asymptotically, we expect the following:

$$SR_1 \to 1-; \qquad SR_0 \to 0+. \quad (11)$$

TABLE III. Cross sections and the optical point following from models $mBP1$ and $mBP2$.

Model	$\sqrt{s}$ (GeV)	$\sigma_{\rm tot}$ (mb)	$\sigma_{\rm el}$ (mb)	$d\sigma_{\rm el}/dt\|_{t=0}$ (mbGeV^{-2})
$mBP1$	24	40.0	6.80	82.0
	31	40.6	7.15	84.3
	45	42.1	7.14	90.9
	53	42.9	7.43	94.0
	63	43.7	7.68	97.8
	7000	101	25.6	524
$mBP2$	24	37.9	6.65	73.6
	31	40.1	7.20	82.4
	45	41.6	7.13	88.7
	53	42.4	7.42	92.1
	63	43.3	7.60	96.3
	7000	100	25.5	515

In order to estimate the values taken by SR_0 and SR_1 and check whether total absorption has been taking place, an estimate for $\hat{\rho}$ is needed. To this aim we use the soft-k_t resummation model of Ref. [21] where the leading term of the cross section is driven by QCD mini-jets. In this model the asymptotic behavior of the total cross section is obtained as $\sigma_{\rm total} \sim (\ln s)^{1/p}$ [22], where the parameter p controls the large-b behavior of the impact-parameter distribution and obeys the constraint $1/2 < p < 1$. Asymptotically then, $\hat{\rho}(s) = \pi/2p \ln s$.

We show in Table IV the numerical results for SR_1 and SR_0 for both models, $mBP1$, where the small $-t$ modification is obtained through a term reflecting the two-pion loop singularity, and $mBP2$, where the form factor is dominating the $t \simeq 0$ behavior. The table indicates that the modified models ameliorate the satisfaction of the sum rules with respect to the simpler BP parametrization, but the asymptotic value $SR_1 = 1$ is not yet reached.

We also notice that in the BP model (and in its modified versions as well), the real-to-imaginary part of the elastic amplitude in the forward direction, $\rho(s)$, is given by

$$\rho(s) = \frac{\hat{\rho} - \sqrt{\left(\frac{C}{A}\right)}\sin\phi}{1 - \sqrt{\left(\frac{C}{A}\right)}|\cos\phi|} \to \hat{\rho} + \sqrt{\left(\frac{C}{A}\right)}[\hat{\rho}|\cos\phi| - \sin\phi], \tag{12}$$

for $\sqrt{C/A} \ll 1$. We shall make use of Eq. (12) when discussing asymptotic predictions.

Before leaving this section, we present the results one obtains when the model $mBP2$ is applied to elastic $\bar{p}p$ data. We show the results of the fits to $\bar{p}p$ data in Fig. 3. Data are from Refs. [23–25] for $S\bar{p}pS$ and from Refs. [26–28] for the Tevatron. We note the absence of a distinctive dip in $\bar{p}p$, but also its faint appearance as the energy increases. From this and other indications, one can argue that, at those energies where $\bar{p}p$ data are available, asymptotia has not yet been reached. For the fits, a value for the parameter t_0 in the form factor needs to be chosen. Interpolating between ISR and the LHC, we obtain for t_0 the values indicated in the figure. At the end of this paper, we shall comment more on the differences between the energy behavior of the parameters for pp and $\bar{p}p$.

TABLE IV. Sum rules for modified BP models at ISR23, ISR53 and LHC7.

Model	p	$\sqrt{s}$ (GeV)	SR_1	SR_0
$mBP1$	…	24	0.721	0.011
	…	53	0.722	0.049
	0.66	7000	0.953	0.067
	0.77	7000	0.956	0.046
$mBP2$	…	24	0.719	0.021
	…	53	0.717	0.049
	0.66	7000	0.950	0.070
	0.77	7000	0.953	0.048

A. Slope parameter in the modified models

The introduction of a *general* factor, $G(s, t)$, given either as in Eq. (A2) or by the square of the proton form factor, leads to a change of curvature in the local slope. This behavior should be expected since the new model is influenced by $G(s, t)$ as follows:

$$B_{\rm eff}(s,t) = \left(\frac{d\sigma_{\rm el}}{dt}\right)^{-1}\Big[ABe^{Bt}G^2(s,t) + 2Ae^{Bt}G(s,t)\frac{dG(s,t)}{dt} + CDe^{Dt} + \sqrt{AC}(B+D)G(s,t)e^{(B+D)t/2}\cos\phi + 2\sqrt{AC}e^{(B+D)t/2}\frac{dG(s,t)}{dt}\cos\phi\Big]. \tag{13}$$

In Fig. 4 we display data for the effective forward slope $B_{\rm eff}(s) \equiv B_{\rm eff}(s, t = 0)$, compared with the local slope $B_{\rm eff}(s, t)$, at ISR53 and LHC7, following from the above-mentioned models. We notice from this figure that the modification with the square root in the exponential, $mBP1$, appears to overrate near-forward slopes. In fact, the respective forward slopes exceed by some 10% the measurements at ISR53 and LHC7. This provides yet another reason to focus on the form-factor-modified model,

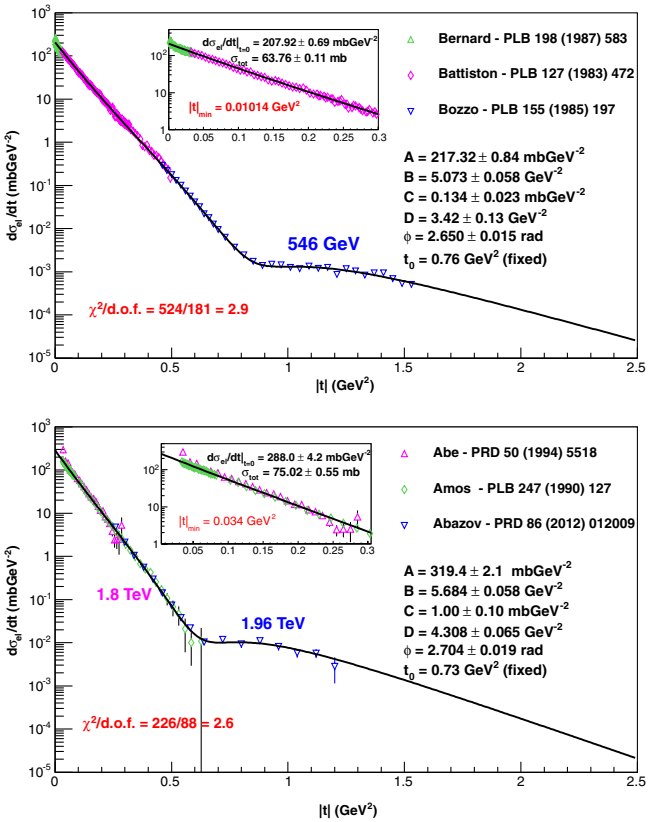

FIG. 3 (color online). The $mBP2$ model applied to $\bar{p}p$ data. The values for parameters thus obtained are shown in the plots.

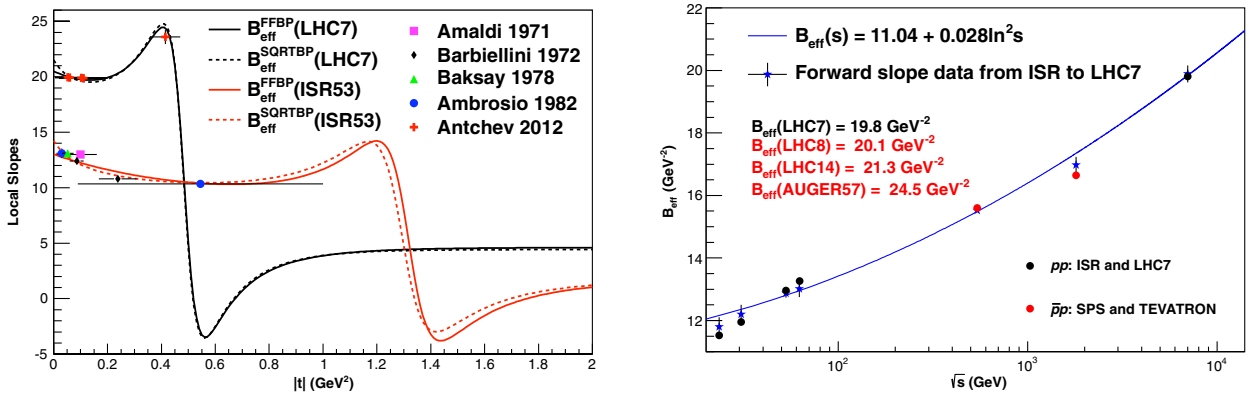

FIG. 4 (color online). Left: Local and forward slopes from the two-pion threshold model (dashes, label $B_{\rm eff}^{\rm SQRTBP}$) and the form factor one (full line, label $B_{\rm eff}^{\rm FFBP}$) at ISR53 and LHC7. Right: The effective forward slope from both pp and $\bar{p}p$ data (blue stars). Data are compared with a fit in $(\ln s)^2$ and from the model approximation of Eq. (14), using results from Table II for pp (black dots). Red dots indicate the result for $\bar{p}p$, with the scale t_0 as in Fig. 3.

*mBP*2. We also notice that, from a numerical point view, while in the original BP model $B(s) \simeq B_{\rm eff}(s)$, in the case of *mBP*2 the following approximation holds:

$$B(s) \simeq B_{\rm eff}(s) - \frac{8}{t_0}, \tag{14}$$

as one can easily check using Eq. (13). For this model, we also show in the right panel of Fig. 4 the comparison between $B_{\rm eff}(s)$ from experimental results from ISR to LHC. The parametrization applied in Fig. 4 for $B_{\rm eff}(s)$ is inspired by the asymptotic theorems, and is consistent with the result for the effective slope by Schegelsky and Ryskin [29]. Indeed, when fitting $B_{\rm eff}(s)$ with an additional term with a linear $\ln s$ dependence, the respective coefficient is consistent with zero. This leads to the best fit shown in Fig. 4, with $B_{\rm eff}(s) \sim (\ln s)^2$.

IV. ASYMPTOTIC PREDICTIONS OF THE EMPIRICAL MODEL *mBP*2

The original BP model of Eq. (1) had purported to present a "model independent analysis of the structure in pp scattering" [3]. As such, and as pointed out by Uzhinsky and Galoyan [30], the BP parametrization does not, in itself, possess a predictive power. However, its simplicity can be exploited to make higher-energy predictions. In fact, the model has the virtue of allowing a simple implementation of the asymptotic sum rules we presented in Ref. [4], and thus to obtain the asymptotic behavior of the parameters which can lead to the predictions of the present model for the elastic differential cross section at LHC8 and LHC14. We shall now proceed to illustrate such an asymptotic, and partly empirical, realization of the *mBP*2 model.

This model has six parameters, i.e. two amplitudes $\sqrt{A(s)}$ and $\sqrt{C(s)}$, two slopes $B(s)$ and $D(s)$, a phase ϕ and a scale t_0. The fits to ISR and LHC7 data suggest $t_0 \to 0.71$ GeV^2 at LHC energies, and thus for asymptotic predictions we fix t_0 to acquire the value of the EM form factor of the proton, i.e. $t_0 = 0.71$ GeV^2. As for the phase ϕ, the same fits support the approximation $\phi \sim$ const in energy. In Regge models, the phase would be t dependent, and, in such case, the phase, as used here in the empirical model, would represent a value averaged over the range Δt of validity of this model.

Having thus made the ansatz that both t_0 and ϕ are asymptotically constant, we remain with four energy-dependent parameters. As we shall shortly discuss in detail, to comply with asymptotic theorems $\sqrt{A(s)}$ and $B(s)$ should have the same asymptotic behavior, namely at most like $(\ln s)^2$. For the slope of the second (nonleading) term, an asymptotic normal Regge behavior would be the most appealing possibility. The amplitude of the second term is so far unconstrained. From the asymptotic sum rules, the amplitude $\sqrt{C(s)}$ can either have a constant or a logarithmic energy dependence. We shall now see how this behavior can be understood in more detail.

The satisfaction of the sum rules for elastic scattering at higher energies, namely, $SR_1 \to 1$ and $SR_0 \to 0$, is suggested by our results, presented in Table IV. Based on their saturation, we propose to make predictions concerning the energy behavior of the parameters $A(s)$, $B(s)$, $C(s)$ and $D(s)$. We begin with the simple BP model, which contains the asymptotics of the sum rules, since both $\gamma(s)$ and t_0 of the modified versions of the model are approximately constant in energy. The asymptotic sum rules read

$$SR_0 = \sqrt{\frac{A(s)}{1+\hat{\rho}(s)^2}}\frac{\hat{\rho}(s)}{\sqrt{\pi}B(s)} - \frac{\sqrt{C(s)}\sin\phi}{\sqrt{\pi}D(s)} \to 0, \tag{15}$$

$$SR_1 = \sqrt{\frac{A(s)}{1+\hat{\rho}(s)^2}}\frac{1}{\sqrt{\pi}B(s)} + \frac{\sqrt{C(s)}\cos\phi}{\sqrt{\pi}D(s)} \to 1. \tag{16}$$

Since ϕ is approximately constant throughout the range from ISR and beyond, and if $\hat{\rho}(s) \sim 1/\ln s$, one can then

obtain the following asymptotic relationships between the parameters:

$$\frac{\sqrt{A(s)}}{B(s)} \sim \frac{\sqrt{C(s)}}{D(s)} \ln s, \tag{17}$$

$$\frac{\sqrt{A(s)}}{B(s)} \sim \frac{\sqrt{\pi}}{(1+\frac{\pi \cot\phi}{2p \ln s})} \sim \text{const}, \tag{18}$$

where s, the squared c.m. energy, is meant to be in units of GeV^2.

We now start from the fact that to leading order in $\ln s$, the parameter $A(s) \propto \sigma_{\text{tot}}^2$. The satisfaction of asymptotic theorems [31] suggests that asymptotically $\sigma_{\text{total}} \sim B(s)$, which is also in agreement with Eq. (18).

We consider here a specific realization of the Froissart-Martin bound [6,7], namely the case of maximal *energy* saturation. The more general case of $\sigma_{\text{total}} \sim (\ln s)^{1/p}$ with $1/2 < p < 1$ will be discussed elsewhere. Then,

$$A(s) \sim (\ln s)^4, \qquad B(s) \sim (\ln s)^2, \qquad D(s) \sim \sqrt{C(s)} \ln s. \tag{19}$$

The above results are proposed in the context of the simple BP model, with five parameters. The form-factor modification of Eq. (3) may introduce some changes, but, if we assume the parameter t_0 to asymptote to a constant value (of $t_0 \simeq 0.71\ \text{GeV}^2$), its introduction will not spoil the simple relations of Eqs. (17) and (18). We point out that the ansatz $B(s) \sim (\ln s)^2$ is asymptotically consistent with data, as discussed in Ref. [29] and seen in Fig. 4. However, at nonasymptotic energies the parameter $B(s)$ may have a slower growth.

To estimate the energy dependence of the parameters of the nonleading term, i.e. $D(s)$ and $C(s)$, is more complicated. An important consequence of Eq. (12) is that $\sqrt{C(s)}$, if at all, must increase less than $\ln s$, if both $\rho(s)$ and $\hat{\rho}(s) \sim (\ln s)^{-1}$ asymptotically. Namely, we have the following:

(i) If the first term, $\sqrt{A(s)}$, in the elastic amplitude indeed represents a $C = +1$ vacuum term, then

$$\hat{\rho}(s) \to \frac{\pi}{\ln s}. \tag{20}$$

(ii) If the Froissart-Martin bound is indeed saturated, then we have the Khuri-Kinoshita theorem according to which also

$$\rho(s) \to \frac{\pi}{\ln s} [\text{with the same coefficient } \pi]. \tag{21}$$

(iii) If both Eqs. (20) and (21) are simultaneously true, then we must have that

$$[\sqrt{(C/A)}] \ln(s) \to 0. \tag{22}$$

(iv) The above precludes $\sqrt{C(s)}$ from growing asymptotically as $\ln(s)$, if $\sqrt{A(s)} \sim [\ln(s)]^2$.

In the logarithmic approximations we are using here, the simplest assumption—albeit not the only one—satisfying the sum rules, the Froissart bound and the Khuri-Kinoshita theorem [8] is then

$$D(s) \sim \ln s, \qquad \sqrt{C(s)} \sim \text{const}. \tag{23}$$

In other words, when the Khuri-Kinoshita asymptotic behaviour for the real part of the amplitude is satisfied, one can choose the amplitude $C(s) \to$ const and the sum rules dictate a normal Regge-like behavior for the slope of the nonleading term, $D(s)$. However there are some caveats and subtleties to be aware of:

(i) The phenomenology presented for pp, and $\bar{p}p$ scattering as well, shows that $\sqrt{C(s)}$ increases very rapidly from ISR to LHC7, and hence a constant behavior over this energy range is not observed (see Table II).

(ii) For a large range of the energy interval $\rho(s) \sim$ const [average value 0.12] and thus over the same range $C(s)$ may increase in order to keep $SR_0 \sim 0$. This seems to be borne out by the phenomenology.

Thus it is quite possible that, at least in the energy range in which $\rho(s) \sim$ const, $\sqrt{C} \sim \ln(s)$. Unfortunately, with present data, no unique limit can be prescribed. We shall thus resort to an empirical parametrization for $\sqrt{C(s)}$, as shown shortly below.

A. Phenomenological results for the parameters and their physical meaning

In this section we propose an empirical description of the differential elastic pp cross section to be used at LHC8 and LHC14. This parametrization follows Eq. (3) and refines the one proposed in Ref. [4], presenting an optimal description of the very small $-t$ value, in addition to the already mentioned good description of the dip and the tail.

Following the above discussion, and fits to ISR and LHC7 data we propose the following asymptotic parametrization:

$$4\sqrt{\pi A(s)}(mb) = 47.8 - 3.8 \ln s + 0.398(\ln s)^2, \tag{24}$$

$$\begin{aligned} B(s)(\text{GeV}^{-2}) &= B_{\text{eff}}(s) - \frac{8}{t_0} \\ &= 11.04 + 0.028(\ln s)^2 - \frac{8}{0.71} \\ &= -0.23 + 0.028(\ln s)^2, \end{aligned} \tag{25}$$

$$4\sqrt{\pi C(s)}(\text{mb}) = \frac{9.6 - 1.8 \ln s + 0.01(\ln s)^3}{1.2 + 0.001(\ln s)^3}, \tag{26}$$

$$D(s)(\text{GeV}^{-2}) = -0.41 + 0.29 \ln s. \tag{27}$$

The parametrization for $C(s)$ is empirical, $\sqrt{A(s)}$ and $B(s)$ follow asymptotic maximal energy saturation behavior,

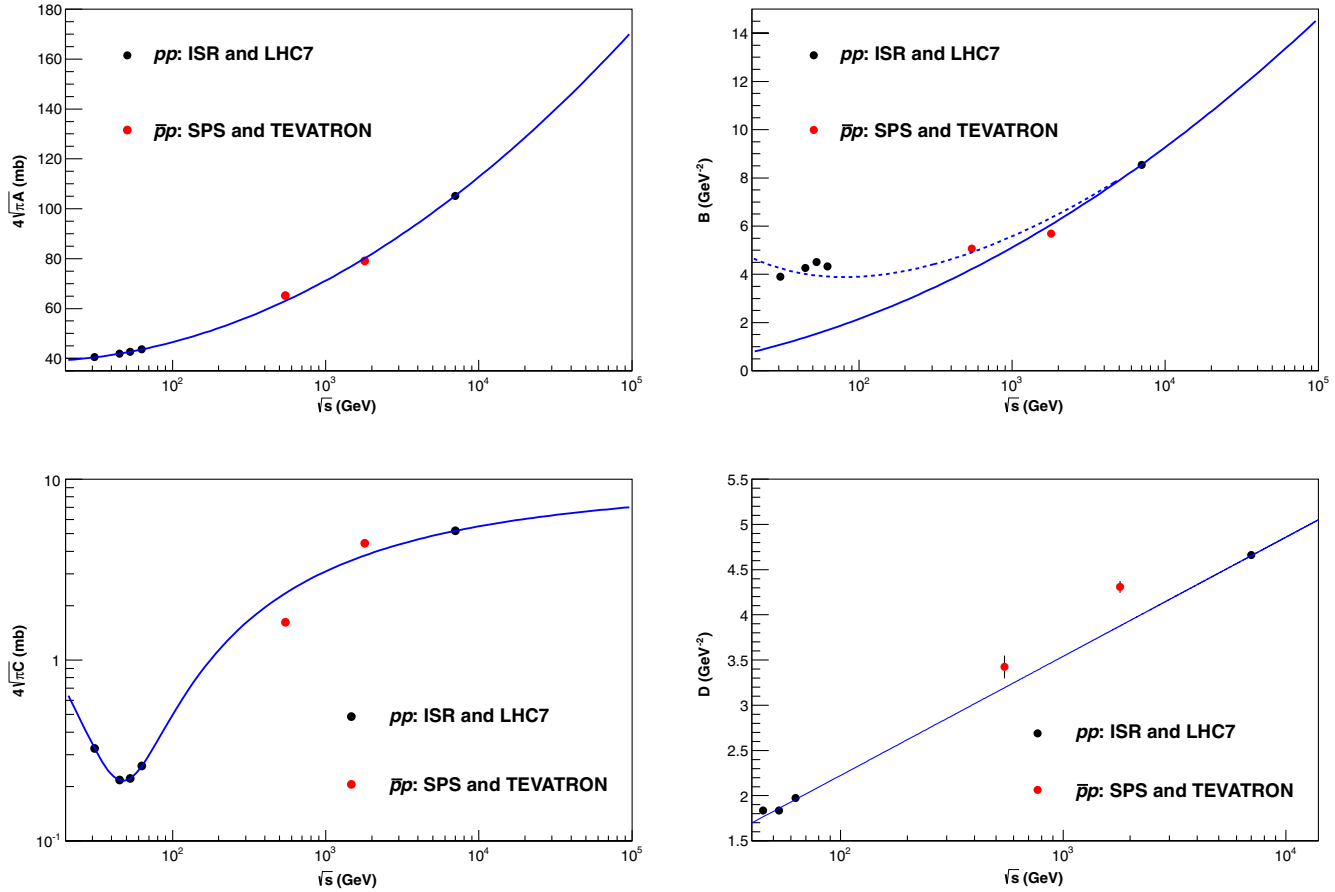

FIG. 5 (color online). Energy behavior of the model parameters $\sqrt{A(s)}$, $B(s)$, $\sqrt{C(s)}$, $D(s)$ described in the text. Black dots correspond to parameter values determined by a fit to pp scattering data. Red dots correspond to the parameter values fitting $\bar{p}p$ data, and were not used to determine the parametrization given in Eqs. (24)–(27). The indicated parametrizations follow asymptotic sum rules and theorems and cannot expect to be valid for lower ISR energies. The dashed curve in the $B(s)$ panel accounts for the behavior of t_0 at nonasymptotic energies.

and $D(s)$ shows normal Regge behavior. In Fig. 5 we plot the parametrizations from Eqs. (24)–(27), and indicate the results of the fit to the elastic differential cross sections for pp data (black dots). The red dots indicate the value of the parameters obtained when fitting $\bar{p}p$ data with the $mBP2$ model. Notice that $\bar{p}p$ data were not used to determine the parametrization given in Eqs. (24)–(27). A comment on the difference between the results of the fit of pp and $\bar{p}p$ can be found in the next section.

B. A simple Regge-model for constant average ϕ

We have mentioned that, for the purpose of the empirical parametrization described by this model, the phase ϕ is to be considered as averaged over the range of momentum transfer under consideration. The previous phenomenology also indicates that it is approximately constant in energy. Here we shall show the connection between an arbitrary phase such as ϕ and the contribution to the amplitude from $C = \pm 1$ states, commenting on the energy dependence. This follows if, in Regge language, the two trajectories contributing to the amplitude are degenerate.

Consider a $C = +1$-state contribution to the elastic amplitude. It reads

$$\mathcal{A}_R^{(+)}(s,t) = iC_+\left(\frac{1}{s}\right)\left[\left(\frac{se^{-i\pi/2}}{s_o}\right)\right]^{\alpha_+(t)}, \qquad (28)$$

where $\alpha_+(t)$ is the positive-signature trajectory, R stands for a general Regge parametrization, and s_o is a generic energy scale. For a $C = -1$ state, on the other hand, we have

$$\mathcal{A}_R^{(-)}(s,t) = C_-\left(\frac{1}{s}\right)\left[\left(\frac{se^{-i\pi/2}}{s_o}\right)\right]^{\alpha_-(t)}, \qquad (29)$$

where $\alpha_-(t)$ is the negative-signature trajectory. Notice, the absence of i in the second term.

We consider the two trajectories to be degenerate (in analogy to the often invoked "standard" exchange degeneracy between f_2-a_2 and ρ-ω trajectories, which is so essential for a lack of resonances in "exotic" channels). Consider the limit

$$\alpha_+(t) = \alpha_-(t). \qquad (30)$$

If as usual we assume them to be linear and just for simplicity also assume that $\alpha_{\pm}(0) = 1$ (the case of the "old" uncritical Pomeron), we may write their total contribution as

$$\mathcal{A}_R(s,t) = i\frac{C_+ - iC_-}{s_o} e^{t\alpha'(ln(s/s_o)-i\pi/2)}. \quad (31)$$

If we define

$$C_+ = s_o C\cos\phi; \qquad C_- = -s_o C\sin\phi, \quad (32)$$

we may rewrite Eq. (31) as

$$\mathcal{A}_R(s,t) = iCe^{t\alpha'(ln(s/s_o)-i\pi/2)}e^{i\phi}. \quad (33)$$

Apart from the "extra" phase $e^{-it\alpha'\pi/2}$, this corresponds to the second term of the Barger-Phillips amplitude, the "C-term." Notice that this phase is present in any Regge amplitude.

Now we turn to some numerics related to this identification. Clearly, $D(s) = 2\alpha' \ln(s/s_o)$. Our phenomenological value gives approximately $D(s) \approx 0.29 \ln(s/s_o)$ GeV^{-2}, which corresponds to $\alpha' \sim 0.145$ GeV^{-2}. This "extra" phase $\Delta(t) = -t\alpha'\pi/2$ [which is constant in s and hence nonleading with respect to $\ln(s/s_o)$] in our case is bounded between $0 < \Delta(t) < 0.23$ as $0 < |t| < 1$ GeV^2, an order of magnitude smaller than the values of $\phi = 2.7 \div 2.9$ rad found.

Figure 5 shows that the fit values for $C(s)$ and the slope $D(s)$ for $\bar{p}p$ scattering do not completely follow the parametrization obtained for the case of pp amplitudes. In Regge language, this corresponds to different nonleading contributions from the Regge trajectories. The essential point is that while the leading terms for pp and $\bar{p}p$ are the same by virtue of asymptotic theorems, the nonleading terms [characterized by $C(s)$, $D(s)$ and the phase] are not, leading to different ratios of charge-conjugation $C = \pm 1$ terms for the two cases. In this paper we shall not discuss this point further, leaving a Regge analysis of this model to future studies.

C. The position of the dip

Although the phase ϕ is consistent with a constant as the energy increases, its value fluctuates. In the range $\sqrt{s} = 53$–7000 GeV, the fits for pp and $\bar{p}p$ indicate $\phi \simeq 2.7 \div 2.9$ rad. We note that the value used for ϕ influences the position and depth of the dip. In order to choose a value for ϕ, we then study how the dip moves as a function of energy. The simplest asymptotic assumption for the dip position as a function of energy is to assume geometrical scaling, namely $t_{\rm dip}\sigma_{\rm total} \sim$ const. In the maximal saturation model, in which $\sigma_{\rm total} \sim (\ln s)^2$, one can then parametrize the dip position as

$$t_{\rm dip} = -\frac{a}{1 + b(\ln s)^2}. \quad (34)$$

In Fig. 6 we compare data for the position of the dip in pp scattering with a parametrization obtained from Eq. (34)

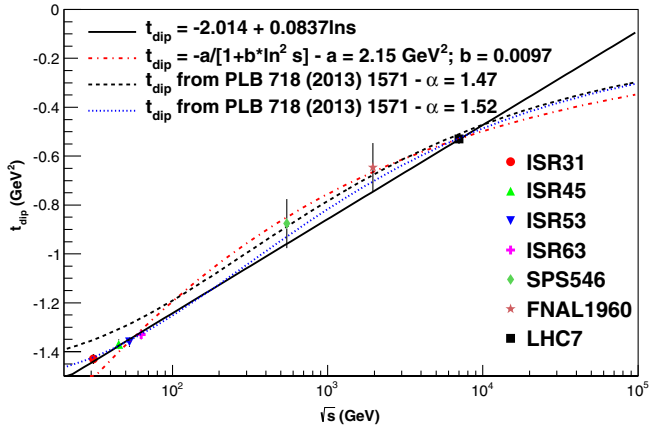

FIG. 6 (color online). Experimental values for the position of the dip in pp and $\bar{p}p$ elastic scattering vs models suggested by geometrical scaling [32] or a simple logarithmic energy rise.

and with other predictions from amplitudes obeying geometrical scaling as discussed in Ref. [32]. A linear logarithmic fit is also shown for comparison. Using these different possibilities, one can calculate the position of the dip at LHC8 and LHC14, as shown in Table V. In this table, $GS1$ refers to the parametrization of Eq. (34), and $GS2$ and $GS3$ refer to different applications of the geometrical scaling model of Ref. [32]. The geometrical scaling values are in good agreement with recent predictions for the dip position at LHC14 from Refs. [33,34].

V. PREDICTIONS FOR LHC8 AND LHC14 AND THE BLACK-DISK LIMIT

We are now in a position to predict the t dependence of the elastic differential cross section in pp scattering at higher LHC energies, using the empirical asymptotic model described in the previous section. In Fig. 7 we show these predictions for pp elastic differential cross sections at LHC8 and LHC14. This model does not include a second dip, or a wiggle, as in many eikonal models, such as that seen in Ref. [35]. On the other hand, at present, at LHC7, in the interval $0 < -t < 2.5$ GeV^2 TOTEM data do not allow one to establish the presence of a second dip or wiggle. Finally, the dotted and full line correspond to different values of the phase ϕ and the figures confirm the sensitivity of the dip depth and position to the chosen value for the phase ϕ.

We now turn to higher energies and consider one favorite test of asymptotia, namely the black disk limit for the ratio

TABLE V. Dip position from $\sqrt{s} = 8$ TeV onwards as predicted by geometrical scaling models and simple linear logarithmic evolution.

$\sqrt{s}$ (TeV)	$\lvert t\rvert^{\rm LIN}_{\rm dip}$	$\lvert t\rvert^{GS1}_{\rm dip}$	$\lvert t\rvert^{GS2}_{\rm dip}$	$\lvert t\rvert^{GS3}_{\rm dip}$
8	0.510	0.518	0.495	0.511
14	0.417	0.471	0.439	0.452

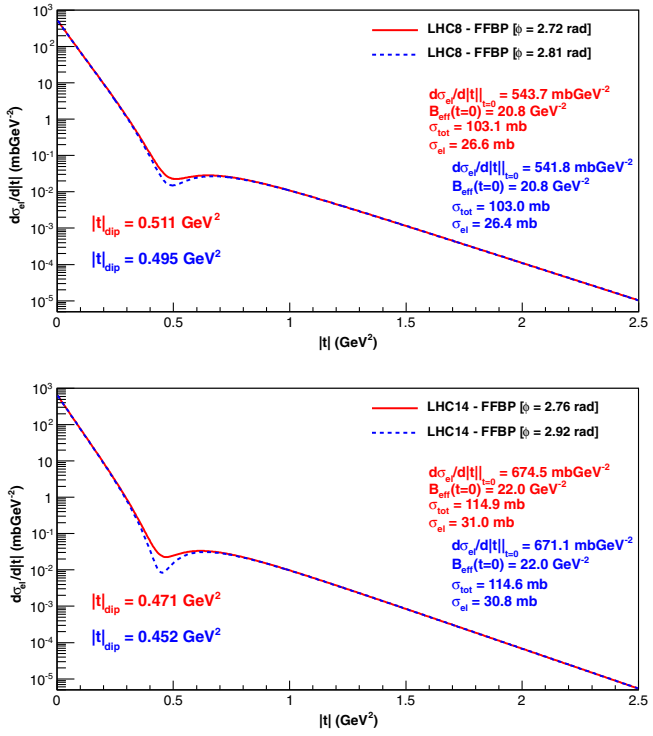

FIG. 7 (color online). *mBP*2 model predictions for the differential elastic cross section at LHC8 and LHC14 in a maximal-energy-saturation model, $\sigma_{\text{total}} \sim (\ln s)^2$.

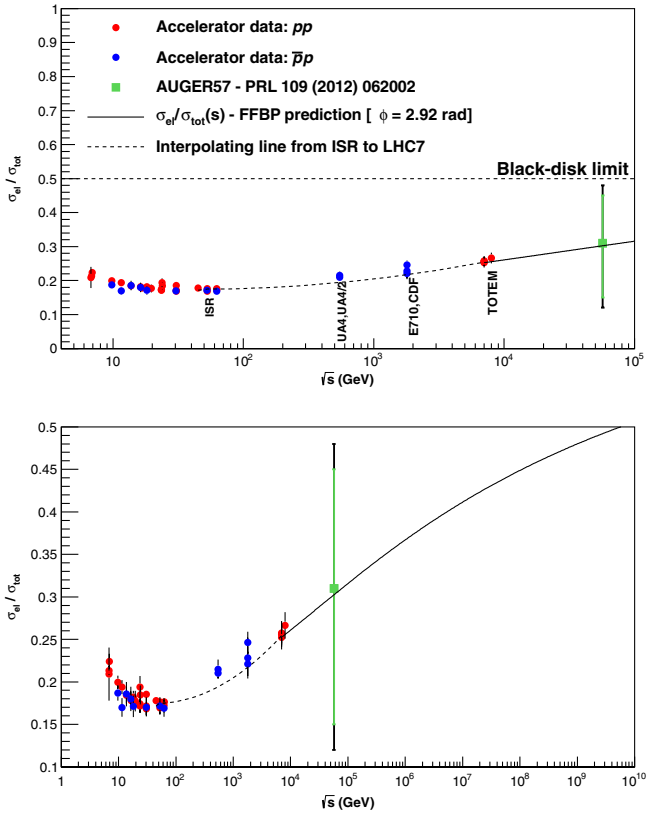

FIG. 8 (color online). Experimental data from accelerators for the ratio $R_{\text{el}} = \sigma_{\text{elastic}}/\sigma_{\text{total}}$ as compiled from Refs. [1,2,38,39] and this model's expectations. The Auger datum has been extracted from the ratio $\sigma_{\text{inel}}/\sigma_{\text{total}}$ at $\sqrt{s} = 57$ TeV, which comes from estimates presented in Ref. [37]. For this point, the inner bars (green) comprise only statistical and systematic uncertainties combined quadratically and the outer bars (black) incorporate the total uncertainty, with errors from Glauber calculations also summed in quadrature. Inner bars: $R_{\text{el}}^{\text{stat+sys}}(57\ \text{TeV}) = 0.31^{+0.14}_{-0.16}$; outer bars: $R_{\text{el}}^{\text{stat+sys+Glauber}}(57\ \text{TeV}) = 0.31^{+0.17}_{-0.19}$.

of the elastic to the total cross section, $R_{\text{el}} = \sigma_{el}/\sigma_{tot}$. As was also noticed in Ref. [36], present data from LHC7 indicate that we are still far from this limit. The question is, how far?

Using the energy parametrization discussed in the previous section, an approximately constant scale t_0 and a band of values for ϕ, we obtain the result shown in Fig. 8. We notice that this ratio is in agreement with Auger results [37]. Moreover, the asymptotic behavior is dictated by the sum rules, which reinforcing the condition of total absorption of partial waves, lead to the saturation of the black-disk limit, i.e. $R_{\text{el}} \to 1/2$ as $s \to \infty$. From the parameters presented in Table VI, we estimate that $R_{\text{el}} \simeq 1/2$ at $\sqrt{s} \simeq 10^{10}$ GeV (corresponding to the energy in the lab frame $E \simeq 10^{20}$ GeV), i.e. at energies typically larger than the Planck scale.

As expected, the ratio R_{el} is less sensitive to variations in ϕ, since the contribution arising from the dip region to the integrated elastic cross section is minimal. Therefore, notwithstanding the observable effect in the elastic differential cross section, shown in Fig. 7, the predictions of this model for different values of ϕ lead to practically overlapping curves.

We now summarize the physics content of the proposed parametrization as follows:

(1) The first term in which the amplitude is split corresponds to a leading positive charge-conjugation term, $C = +1$, and the second term corresponds to a mixture of $C = +1$ and $C = -1$ exchanges. The value of the phase, $\phi \sim \pi$ but $\neq \pi$, $\pi/2$ indicates that the second term is predominantly $C-$ even, and thus the interpretation of the tail as due only to a three-gluon exchange [19] is not observed in this model.

(2) The parameters of the first term control the total cross section, via $A(s)$, and the diffraction peak with $B(s)$; the parametrization of their energy behavior is valid for both pp and $\bar{p}p$. This is in keeping with the Pomeranchuk theorem.

(3) For the second term, the slope $D(s)$ can be interpreted as arising from nonleading Regge and Pomeron exchanges. These contributions differ for pp and $\bar{p}p$. This is confirmed by the fact that its energy behavior is not quite the same for the two processes. A similar argument can be used for the energy dependence of the nonleading amplitude $C(s)$, which is a mixture of $C-$ even and $C-$ odd exchanges.

TABLE VI. Values of $mBP2$ parameters used in the predictions at LHC8, LHC14 and AUGER57 and the ratio $R_{\rm el}$ at each c.m. energy. In all cases the values of t_0 have been frozen at 0.71 GeV^2 and bands for ϕ were considered. These bands determine the uncertainty in the predictions for the ratio.

$\sqrt{s}$ (TeV)	A (mbGeV^{-2})	B (GeV^{-2})	C (mbGeV^{-2})	D (GeV^{-2})	ϕ (rad)	$\sigma_{\rm el}/\sigma_{\rm tot}$
8	596	8.8	1.44	4.7	2.72–2.81	0.257 ± 0.001
14	739	10.0	1.70	5.1	2.76–2.92	0.270 ± 0.001
57	1233	13.2	2.30	5.9	2.72–2.92	0.304 ± 0.001

(4) The proton form factor multiplying the first term is used to describe the probability that the proton does not break up at $-t \simeq 0$.

VI. CONCLUSIONS

We have shown that the pp differential elastic cross section in the range measured by the TOTEM experiment at LHC can be parametrized through two exponentials and a phase, provided the first term is modified by a multiplicative factor to optimize the description of the forward peak. Two different modifications were proposed. For the model with a proton form factor to modify the $-t \simeq 0$ behavior, we extracted predictions at LHC8 and LHC14, and calculated the ratio of the elastic to the total cross section up to and beyond $\sqrt{s} = 57$ TeV.

The parametrization of pp elastic cross-section data presented in this paper is not meant to be exact, but rather to indicate how to break up the amplitude in a set of building blocks, and apply this dissection to the data as the energy increases. This parametrization addresses the following basic elements:

(i) the value of the differential cross section at $t = 0$, namely the optical point value;
(ii) a rapid decrease, characterized by a slope, which, between $-t = 0$ and the dip, is not a constant;
(iii) the occurrence of a dip in pp at all energies from ISR to LHC;
(iv) an exponential decrease after the dip, with a nonleading slope and an amplitude much smaller than before the dip.

This behavior is described by an empirical model, with two amplitudes, two different slopes, a phase and the proton form factor to multiply the amplitudes. This empirical model might help us to understand the elastic pp differential cross section [40]. It describes the data well and, as such, can be used by model builders and experimentalists alike.

The interpretation of the model is in parts straightforward, but not completely. In our previous analysis of TOTEM data for the elastic differential cross section [4], we have commented on the physical meaning of the model. Our considerations were that the two terms in the amplitude receive contributions from different charge-conjugation processes: the first term is purely from $C = +1$, while the second nonleading term has contributions from both $C = \pm 1$ terms, which, at high energies, render $\phi \neq \pi$, $\pi/2$. The energy behavior of the leading amplitude $A(s)$ is consistent with many eikonal models, but the exponential behavior in the momentum transfer before and after the dip is not, and it is probably due to rescattering effects in the final state. On the other hand, the modification of the model with a form factor which reproduces the proton electromagnetic form factor at high energy suggests the need to include rescattering effects within each colliding hadron, namely the probability that the proton does not break up as the momentum transfer increases.

ACKNOWLEDGMENTS

We thank L. Jenkovszky, M. J. Menon and J. Soffer for useful discussions. A. G. acknowledges partial support by Spanish MEC (FPA2010-16696, AIC-D-2011-0818) and by Junta de Andalucia (FQM 6552, FQM 101). D. A. F. acknowledges the São Paulo Research Foundation (FAPESP) for financial support (contract: 2012/12908-4). G. P. thanks the MIT Center for Theoretical Physics for hospitality, and Y. N. S. thanks Northeastern University Physics Department.

APPENDIX A: TWO-PION THRESHOLD EFFECTS ON THE BP MODEL: *MBP1*

We discuss here a model where the very small $-t$ behavior is influenced by the nearest t-channel singularity of the scattering amplitude. In this model, which we call $mBP1$,

$$\mathcal{A}(s,t) = i[\sqrt{A(s)}e^{B(s)t/2}G(s,t) + e^{i\phi}\sqrt{C(s)}e^{D(s)t/2}], \quad \text{(A1)}$$

with $G(s,0) = 1$ in order to not spoil the good description of the dip by Eq. (1), as discussed in the text. Such a factor would arise from the contribution of the *two-pion loop* in the Pomeron trajectory, as was originally proposed in Refs. [10,11], and more recently discussed by Khoze, Martin and Ryskin [12] and Jenkovszky [13,41]. In particular $\alpha_P(t)$, at very small t, should include a square-root singularity at $t = 4\mu^2$, with $\mu = m_\pi$ being the pion mass. Mindful of such possibilities, we have applied the following correction to the first term of Eq. (1), namely we shall use

$$G(s,t) = e^{-\gamma(s)(\sqrt{4\mu^2 - t} - 2\mu)}, \quad \text{(A2)}$$

with $\gamma(s)$ a free parameter. Being applied to the near-forward region, such a term shall influence the small-$|t|$

TABLE VII. Values of the free fit parameters A, B, C, D, γ and ϕ at each energy analyzed. A and C are expressed in units of mbGeV^{-2}, B and D in units of GeV^{-2}, γ in units of GeV^{-1} and ϕ in radians.

$\sqrt{s}$ (GeV)	A	B	$C(\times 10^{-3})$	D	γ	ϕ	$\frac{\chi^2}{\text{d.o.f.}}$
24	82.8 ± 1.0	6.3 ± 0.1	2.3 ± 0.2	1.79 ± 0.04	2.15 ± 0.07	2.94 ± 0.01	$\frac{200}{134-6} = 1.1$
31	85.1 ± 0.2	6.99 ± 0.06	1.9 ± 0.1	1.79 ± 0.02	1.79 ± 0.03	3.02 ± 0.01	$\frac{310}{206-6} = 1.6$
45	91.5 ± 0.2	7.51 ± 0.05	1.18 ± 0.06	1.62 ± 0.02	1.92 ± 0.03	2.73 ± 0.02	$\frac{801}{207-6} = 4.0$
53	94.6 ± 0.1	7.78 ± 0.05	1.49 ± 0.05	1.70 ± 0.01	1.79 ± 0.02	2.68 ± 0.01	$\frac{1490}{319-6} = 4.8$
63	98.5 ± 0.2	7.98 ± 0.09	1.7 ± 0.1	1.75 ± 0.03	1.74 ± 0.04	2.75 ± 0.03	$\frac{332}{165-6} = 2.1$
7000	565 ± 2	13.7 ± 0.2	970 ± 40	4.43 ± 0.03	2.01 ± 0.06	2.703 ± 0.007	$\frac{497}{161-6} = 3.2$

behavior of the elastic differential cross section, producing a changed curvature in the effective slope $B_{\text{eff}}(s, t)$ in this region. The original expressions for the total cross section and the optical point remain unchanged, but the modification of the model of Eq. (1) given by Eqs. (A1) and (A2) introduces an additional t dependence in the first term, through a square root, and hence a sixth parameter. Using the modified BP model of Eqs. (A1) and (A2), we update our fits [4] to LHC7 data samples as well as to the ISR data sets in the full range for pp data with $\sqrt{s} = (23 \div 63)$ GeV, as displayed in Table VII and Fig. 9. ISR data sets used in the fits comprise the data collection by Amaldi and Schubert [14] and all experimental information available from 1980 onwards [15–18]. This table shows that this

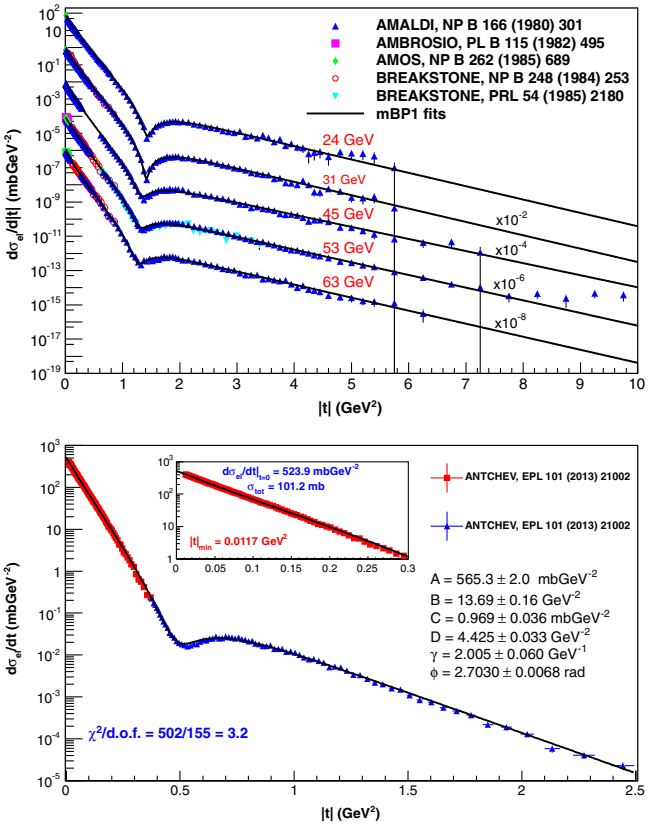

FIG. 9 (color online). Fits to the ISR and LHC7 data sets with the model $mBP1$.

modification gives an acceptable statistical description from the optical point to the full $|t|$ range. In Fig. 10 we present the energy dependence of the fit parameters for the $mBP1$ model. The continuous (dotted) lines in these figures are computer parametrizations drawn to guide the eye.

We now make two comments. Firstly, the square-root factor is only used for the first term of the BP amplitude, as this factor comes from the contribution of the pion loop to the leading vacuum term and it may not be present for the second nonleading term, which, for a generic ϕ, also has contributions from $C = -1$ processes. The second comment comes from an inspection of Table VII and the energy dependence of the parameter $\gamma(s)$. This energy dependence, displayed in Fig. 10 from ISR to LHC7, shows a very slow increase, even compatible with a constant in energy, shedding doubt on a straightforward interpretation of this factor in terms of a small-t contribution to the Pomeron trajectory.

The elastic cross section for this model from Eqs. (A1) and (A2) is obtained as

$$\sigma_{\text{el}}(s) = \int_{-\infty}^{0} dt |\mathcal{A}(s, t)|^2 = A e^{4m_\pi \gamma} I_1 + \frac{C}{D} + 2\sqrt{AC} e^{2m_\pi \gamma} \cos\phi I_3, \tag{A3}$$

where the integrals I_1 and I_3 are given as

$$I_1 = \int_{-\infty}^{0} dt e^{Bt - 2\gamma\sqrt{4m_\pi^2 - t}}, \tag{A4}$$

$$I_3 = \int_{-\infty}^{0} dt e^{(B+D)t/2 - \gamma\sqrt{4m_\pi^2 - t}}. \tag{A5}$$

An analytical evaluation can be obtained, using the result

$$I(\alpha, \beta, \delta) \equiv \int_{-\infty}^{0} dt e^{\alpha t - \beta\sqrt{\delta^2 - t}} = \frac{1}{\alpha} e^{-\delta\beta} - \frac{\beta\sqrt{\pi}}{2\alpha^{3/2}} \times \text{Erfc}[\sqrt{\alpha}(\delta + \beta/2\alpha)] e^{\alpha\delta^2 + \beta^2/4\alpha}, \tag{A6}$$

where $\text{Erfc}(x) = \frac{2}{\sqrt{\pi}} \int_x^\infty e^{-y^2} dy$ denotes the complementary error function. Thus, from Eqs. (A4)–(A6) it follows that

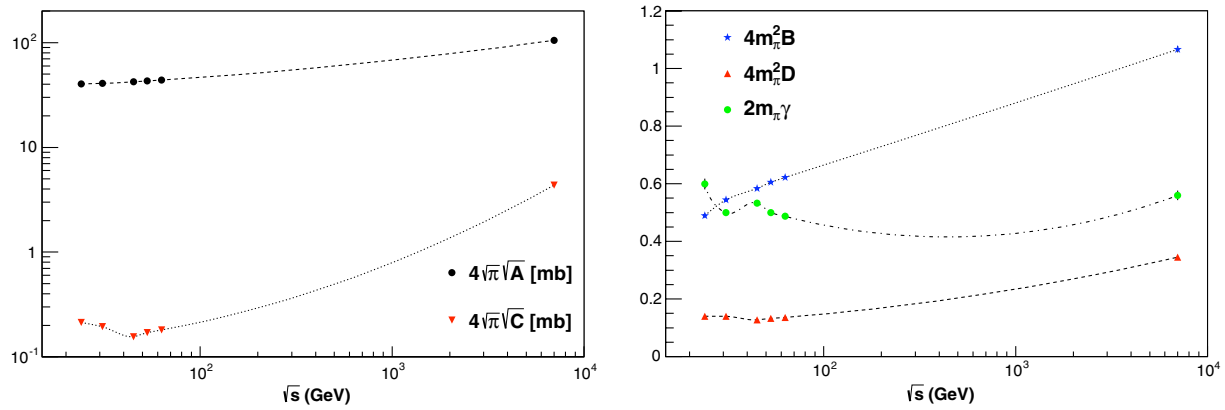

FIG. 10 (color online). Energy behavior of parameters from the $mBP1$ model.

$$\sigma_{\rm el}(s) = \frac{A}{B} + \frac{C}{D} + \frac{4\sqrt{AC}}{(B+D)}\cos\phi - \sqrt{\pi}\frac{A\gamma}{B^{3/2}}\,\mathrm{Erfc}\left[\sqrt{B}\left(2m_\pi + \frac{\gamma}{B}\right)\right]e^{4m_\pi^2(B+\gamma/m_\pi)+\gamma^2/B}$$
$$- \sqrt{8\pi}\frac{\sqrt{AC}\gamma\cos\phi}{(B+D)^{3/2}}\,\mathrm{Erfc}\left[\sqrt{\frac{B+D}{2}}\left(2m_\pi + \frac{\gamma}{B+D}\right)\right]e^{2m_\pi^2(B+D+\gamma/m_\pi)+\gamma^2/2(B+D)}. \quad \text{(A7)}$$

In the above expression one can see that the contributions with positive sign come from the simple BP amplitude, as can easily be checked by taking the limit $\gamma \to 0$. Thus, the presence of negative terms in Eq. (A7), being due to $G(s,t)$, reflects the importance of modifying the first term of the original BP amplitude.

The sum rules for the elastic amplitude presented in Ref. [4] can be applied to this model, and used to check the saturation of the elastic amplitude at LHC energies. One has

$$SR_1 = \frac{1}{\sqrt{\pi}B}\sqrt{\frac{A}{1+\hat{\rho}^2}} + \frac{\sqrt{C}}{\sqrt{\pi}D}\cos\phi - \sqrt{\frac{\pi}{2}\frac{A}{1+\hat{\rho}^2}}\frac{\gamma}{B^{3/2}}\,\mathrm{Erfc}\left[\sqrt{\frac{B}{2}}\left(2m_\pi + \frac{\gamma}{B}\right)\right]e^{2m_\pi^2(B+\gamma/m_\pi)+\gamma^2/2B}, \quad \text{(A8)}$$

$$SR_0 = \frac{\hat{\rho}}{\sqrt{\pi}B}\sqrt{\frac{A}{1+\hat{\rho}^2}} - \frac{\sqrt{C}}{\sqrt{\pi}D}\sin\phi - \hat{\rho}\sqrt{\frac{\pi}{2}\frac{A}{1+\hat{\rho}^2}}\frac{\gamma}{B^{3/2}}\,\mathrm{Erfc}\left[\sqrt{\frac{B}{2}}\left(2m_\pi + \frac{\gamma}{B}\right)\right]e^{2m_\pi^2(B+\gamma/m_\pi)+\gamma^2/2B}. \quad \text{(A9)}$$

As above for the elastic cross section, the first two terms come from the original BP amplitude and the input $G(s,t)$ produces the last term.

APPENDIX B: OTHER FORM-FACTOR MODIFICATIONS OF THE BARGER AND PHILLIPS MODEL

We examine here two more possible modifications of the Barger and Phillips model, complementary to the form-factor modification of the first term, presented in the text.

(i) The entire BP amplitude is multiplied by a factor

$$F_P^2 = \frac{1}{(1 - t/t_0)^4}, \quad \text{(B1)}$$

with t_0 a free parameter, namely

$$\mathcal{A}(s,t) = iF_P^2(t)\Big[\sqrt{A(s)}e^{B(s)t/2} + e^{i\phi(s)}\sqrt{C(s)}e^{D(s)t/2}\Big]. \quad \text{(B2)}$$

(ii) Both terms of the BP amplitude are multiplied by a form factor (squared), but with difference scales, t_0 and t_O, namely

$$\mathcal{A}(s,t) = i\Big[F_P^2(t)\sqrt{A(s)}e^{B(s)t/2} + e^{i\phi(s)}F_O^2(t)\sqrt{C(s)}e^{D(s)t/2}\Big], \quad \text{(B3)}$$

with

$$F_O^2 = \frac{1}{(1 - t/t_O)^4}. \quad \text{(B4)}$$

with $t_{0,O}$ free parameters.

We show the results of the fit in Fig. 11. In Tables VIII and IX we indicate the values taken by the parameters for the best fits of Fig. 11. An inspection of these fits indicates that an overall multiplicative factor, corresponding to the first top plots, is the least favored of the above two possibilities (and less favored than the one chosen in the text, $mBP2$). From the point of view of the χ^2, the fits do not favor the second possibility relative to the choice $mBP2$,

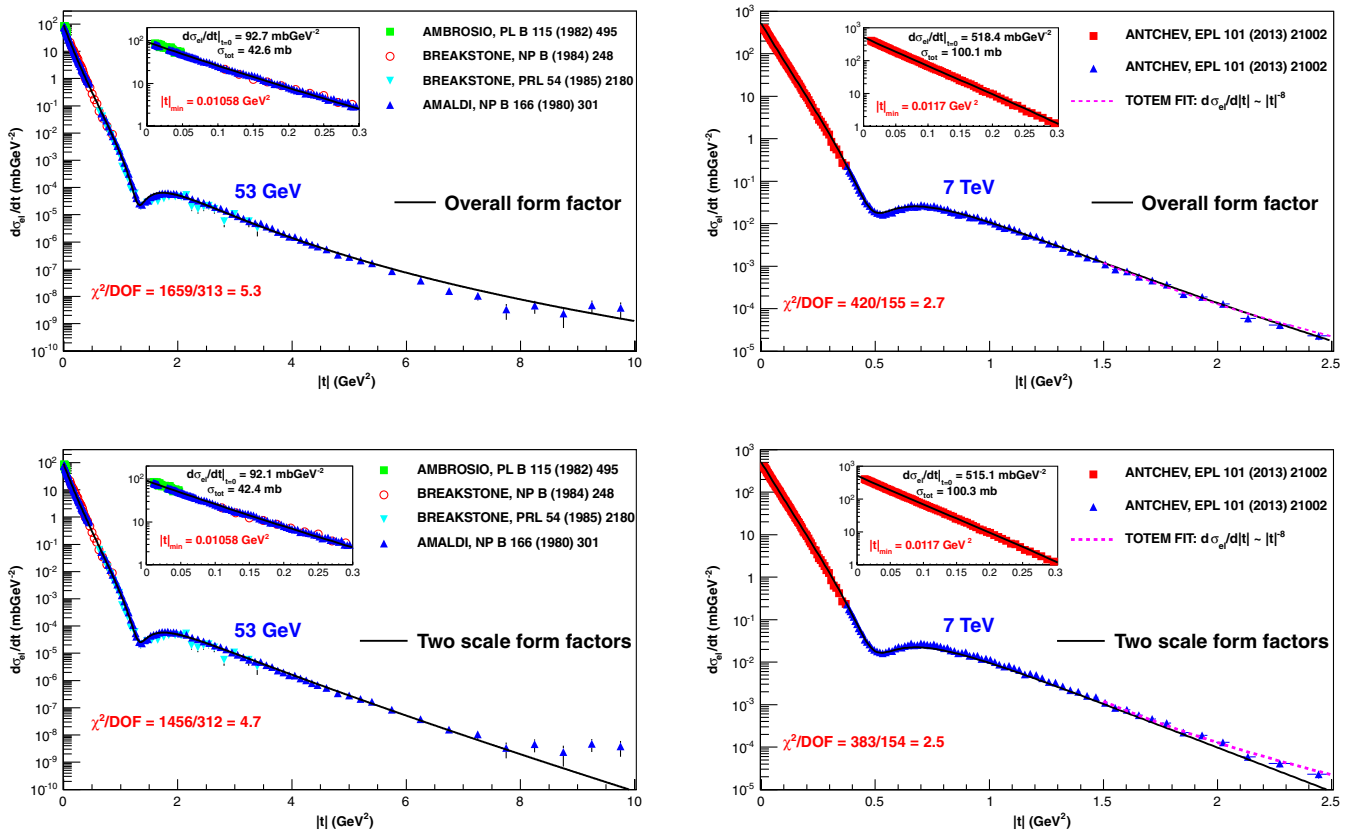

FIG. 11 (color online). Fits to ISR53 and LHC7 data sets with the two other modified BP models described by Eqs. (B2) and (B3), with ISR fits on the left hand side and LHC fits on the right hand side. Top row: BP amplitude multiplied by an overall form factor like term. Bottom row: the two terms in BP amplitude are multiplied by form factors with different scales.

discussed in the text: multiplying both terms by form factors with different scales or only the first term as in $mBP2$, gives an equally good fit, both at ISR and at LHC. However, we notice a problem with the fits of the bottom figures, when the two terms are each multiplied by a different factor, namely these fits are quite insensitive to the second scale. Phenomenologically, therefore, this possibility is not particularly useful, albeit it could be further studied.

APPENDIX C: IMPACT-PARAMETER STRUCTURE IN THE MODIFIED MODELS

Besides the sum rules, the impact-parameter structure of the models $mBP1$ and $mBP2$ provides us useful information about unitarity saturation. From our fits with both models, we extract the elastic profile, through the Hankel transform of the amplitude (A1),

TABLE VIII. Fit parameters of the model with an overall form factor. A and C are in units of mbGeV^{-2}, B and D are in units of GeV^{-2}, ϕ is in radians and t_0 is in units of GeV^2.

$\sqrt{s}$ (GeV)	A	B	C	D	ϕ	t_0	$\frac{\chi^2}{\text{d.o.f.}}$
53	131 ± 2	2.90 ± 0.04	3.4 ± 0.3	0.10 ± 0.01	3.008 ± 0.006	0.811 ± 0.005	$\frac{1659}{319-6} = 5.3$
7000	2180 ± 210	4.3 ± 0.1	580 ± 110	1.54 ± 0.07	3.043 ± 0.007	0.582 ± 0.004	$\frac{420}{161-6} = 2.7$

TABLE IX. Fit parameters of the model with two scale form factors. A and C are in units of mbGeV^{-2}, B and D are in units of GeV^{-2}, ϕ is in radians, and t_0 and t_O are in units of GeV^2.

$\sqrt{s}$ (GeV)	A	B	C	D	ϕ	t_0	t_O	$\frac{\chi^2}{\text{d.o.f.}}$
53	93.3 ± 0.2	4.4 ± 0.1	0.004 ± 0.001	1.1 ± 0.2	2.811 ± 0.02	0.93 ± 0.01	7.2 ± 2.3	$\frac{1456}{319-7} = 4.7$
7000	565 ± 2	8.2 ± 0.2	1.37 ± 0.07	4.65 ± 0.07	2.755 ± 0.008	0.69 ± 0.01	62 ± 247	$\frac{383}{161-7} = 2.5$

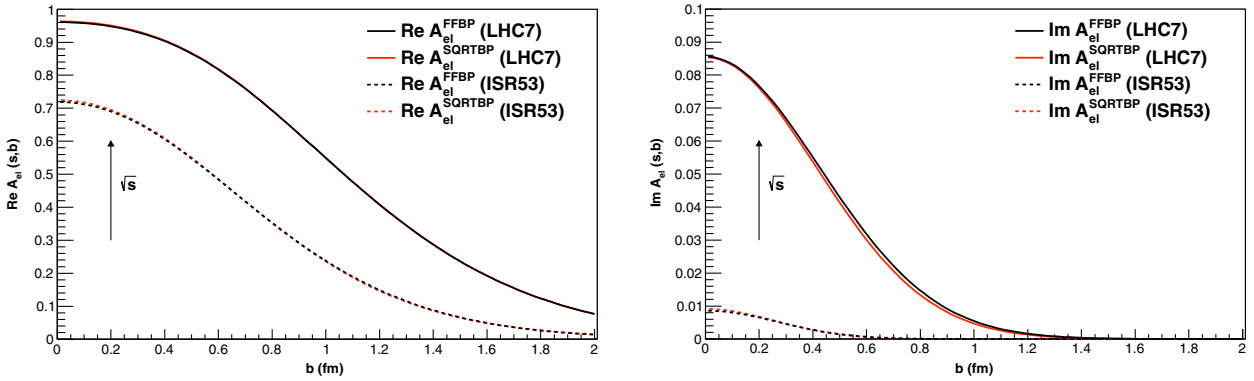

FIG. 12 (color online). Energy evolution of the profile functions (real and imaginary) from ISR to LHC7.

$$\tilde{\mathcal{A}}(s,b) = -i\int_0^\infty qdqJ_0(qb)\mathcal{A}(s,t). \quad \text{(C1)}$$

On the one hand, the dominant contribution comes from the real part, which assumes distinct forms for the models $mBP1$ and $mBP2$,

$$\tilde{\mathcal{A}}_R^{mBP1}(s,b) = \sqrt{A}e^{2m_\pi\gamma}\mathcal{J}(s,b) + \frac{\sqrt{C}}{D}e^{-b^2/2D}\cos\phi, \quad \text{(C2)}$$

$$\mathcal{A}_R^{mBP2}(s,b) = \sqrt{A}t_0^4\mathcal{K}(s,b) + \frac{\sqrt{C}}{D}e^{-\frac{b^2}{2D}}\cos\phi, \quad \text{(C3)}$$

where the integrals $\mathcal{J}(s,b)$ and $\mathcal{K}(s,b)$ are given as

$$\mathcal{J}(s,b) = \int_0^\infty qdqJ_0(qb)e^{-Bq^2/2-\gamma\sqrt{4m_\pi^2+q^2}}, \quad \text{(C4)}$$

$$\mathcal{K}(s,b) = \int_0^\infty qdqJ_0(qb)\frac{e^{-Bq^2/2}}{(t_0+q^2)^4}. \quad \text{(C5)}$$

On the other hand, the imaginary part turns out to be the same,

$$\mathcal{A}_I^{mBP1,mBP2}(s,b) = \frac{\sqrt{C}}{D}e^{-\frac{b^2}{2D}}\sin\phi. \quad \text{(C6)}$$

Unfortunately, due to the introduction of corrections into the first term of the original BP parametrization, the integrals (C4) and (C5) can no longer be solved analytically. Therefore, we perform numerical evaluations of such integrals. In Fig. 12 we present these calculations and the energy evolution of the elastic b distributions, following from Eqs. (C2)–(C6), from ISR energies to LHC7.

[1] G. Antchev *et al.* (TOTEM Collaboration), Europhys. Lett. **101**, 21002 (2013).
[2] G. Antchev *et al.* (TOTEM Collaboration), Phys. Rev. Lett. **111**, 012001 (2013).
[3] R. J. N. Phillips and V. D. Barger, Phys. Lett. **46B**, 412 (1973).
[4] A. Grau, S. Pacetti, G. Pancheri, and Y. N. Srivastava, Phys. Lett. B **714**, 70 (2012).
[5] G. Antchev *et al.* (TOTEM Collaboration), Europhys. Lett. **95**, 41001 (2011).
[6] M. Froissart, Phys. Rev. **123**, 1053 (1961).
[7] A. Martin, Phys. Rev. **129**, 1432 (1963).
[8] N. N. Khuri and T. Kinoshita, Phys. Rev. **137**, B720 (1965).
[9] We note here that an error had occurred in Ref. [4] when fitting ISR data at $\sqrt{s} = 53$ GeV with the inclusion of 63 GeV data in the fit. The conclusions, however, remain unchanged.
[10] G. Cohen-Tannoudji, V. V. Ilyin, and L. L. Jenkovszky, Lett. Nuovo Cimento **5**, 957 (1972).
[11] A. A. Anselm and V. N. Gribov, Phys. Lett. **40B**, 487 (1972).
[12] V. A. Khoze, A. D. Martin, and M. G. Ryskin, Eur. Phys. J. C **18**, 167 (2000).
[13] R. Fiore, L. Jenkovszky, R. Orava, E. Predazzi, A. Prokudin, and O. Selyugin, Int. J. Mod. Phys. A **24**, 2551 (2009).
[14] U. Amaldi and K. R. Schubert, Nucl. Phys. **B166**, 301 (1980).
[15] N. A. Amos *et al.*, Nucl. Phys. **B262**, 689 (1985).
[16] A. Breakstone *et al.* (Ames-Bologna-CERN-Dortmund-Heidelberg-Warsaw Collaboration), Nucl. Phys. **B248**, 253 (1984).
[17] A. Breakstone *et al.*, Phys. Rev. Lett. **54**, 2180 (1985).
[18] M. Ambrosio *et al.* (CERN-Naples-Pisa-Stony Brook Collaboration), Phys. Lett. **115B**, 495 (1982).
[19] A. Donnachie and P. V. Landshoff, arXiv:1309.1292.
[20] A. Donnachie and P. Landshoff, Z. Phys. C **2**, 55 (1979).
[21] R. M. Godbole, A. Grau, G. Pancheri, and Y. N. Srivastava, Phys. Rev. D **72**, 076001 (2005).
[22] A. Grau, R. M. Godbole, G. Pancheri, and Y. N. Srivastava, Phys. Lett. B **682**, 55 (2009).
[23] D. Bernard *et al.* (UA4 Collaboration), Phys. Lett. B **198**, 583 (1987).

[24] M. Bozzo *et al.* (UA4 Collaboration), Phys. Lett. **155B**, 197 (1985).
[25] R. Battiston *et al.* (UA4 Collaboration), Phys. Lett. **127B**, 472 (1983).
[26] V. M. Abazov *et al.* (D0 Collaboration), Phys. Rev. D **86**, 012009 (2012).
[27] F. Abe *et al.* (CDF Collaboration), Phys. Rev. D **50**, 5518 (1994).
[28] N. A. Amos *et al.* (E-710 Collaboration), Phys. Lett. B **247**, 127 (1990).
[29] V. A. Schegelsky and M. G. Ryskin, Phys. Rev. D **85**, 094024 (2012).
[30] V. Uzhinsky and A. Galoyan, arXiv:1210.7338.
[31] M. M. Block and R. N. Cahn, Rev. Mod. Phys. **57**, 563 (1985).
[32] I. Bautista and J. Dias de Deus, Phys. Lett. B **718**, 1571 (2013).
[33] C. Bourrely, J. M. Myers, J. U. Soffer, and T. T. Wu, Phys. Rev. D **85**, 096009 (2012).
[34] E. Ferreira, T. Kodama, and A. Kohara, Eur. Phys. J. C **73**, 2326 (2013).
[35] M. M. Block and F. Halzen, Phys. Rev. D **86**, 014006 (2012).
[36] M. M. Block and F. Halzen, Phys. Rev. D **86**, 051504 (2012).
[37] P. Abreu *et al.* (Pierre Auger Collaboration), Phys. Rev. Lett. **109**, 062002 (2012).
[38] G. Antchev *et al.* (TOTEM Collaboration), Europhys. Lett. **101**, 21004, 2013.
[39] D. A. Fagundes, M. J. Menon, and P. V. R. G. Silva, J. Phys. G **40**, 065005 (2013).
[40] J. Soffer, AIP Conf. Proc. **1523**, 115 (2012).
[41] L. L. Jenkovszky, A. I. Lengyel, and D. I. Lontkovskyi, Int. J. Mod. Phys. A **26**, 4755 (2011).